Aluminum Properties and Physical Metallurgy
John E. Hatch editors, p 25-57
DOI: 10.1361/appm1984p025

CHAPTER 2

CONSTITUTION OF ALLOYS*

Most of the metallic elements readily alloy with aluminum, but only a few are important major alloying ingredients in commercial aluminum-based alloys. Nevertheless, an appreciable number of other elements serve as supplementary alloying additions for improving alloy properties and characteristics.

TYPES OF SYSTEMS

A few generalizations, relating to the periodic system, can be made concerning the types of binary systems the various elements form with aluminum. Beryllium, silicon, zinc, gallium, germanium, tin, and mercury form simple eutectic-type systems with aluminum. Except for beryllium, these elements are in periodic groups IIb, IIIa, and IVa. Cadmium, indium, thallium, and lead of these groups; bismuth of group Va; and sodium and potassium (also probably rubidium and cesium) of group Ia are only partly miscible in liquid aluminum within an appreciable temperature range above its melting point. Therefore, they form simple, monotectic-type systems with aluminum. In binary combinations, aluminum forms no known intermetallic phases or compounds with these elements.

Available data indicate that the remaining metallic elements, including those of the lanthanide and actinide series, are miscible in the liquid state and form more complex binary systems, in which one or more intermetallic phases occur. In these systems, a eutectic reaction generally occurs involving the liquid, the aluminum terminal solid solution, and the aluminum-rich intermetallic phase. However, solid solution is formed near the extreme aluminum end of the system by peritectic reaction between the liquid and the aluminum-rich intermetallic phase with titanium, vanadium, chromium, zirconium, columbium, molybdenum, hafnium, and probably tantalum and tungsten (the elements of groups IVa, Va, and VIa in the fourth, fifth, and sixth periods).

Of the many binary intermetallic phases formed by the reaction of aluminum with the various metallic elements, a few solidify without the occurrence of compositional changes (congruent transformation). However, the majority form a liquid solution of the solid phase composition on cooling, by reaction between a previously existing solid phase and the remaining depleted liquid solution (peritectic reaction). Despite similarities, distinct relationships between the number or types of aluminum intermetallic phases and the elements within a periodic group are difficult to observe.

*This chapter was revised by a team comprised of E.M. Dunn, Kaiser Aluminum & Chemical Corp., *Chairman*; A.P. Davidson, Alcan International Ltd.; J.P. Faunce, Martin Marietta Laboratories; C.G. Levi, ATISA-ATKINS, S.A. de C.V.; S. Maitra, Alcoa Technical Center; and R. Mehrabian, National Bureau of Standards. The original chapter was authored by R.H. Brown and L.A. Willey of Alcoa Technical Center.

Table 1. Invariant Reactions in Binary Aluminum Alloys

Element	Temperature(a) °C	°F	Liquid solubility wt%	at.%	Solid solubility wt%	at.%
Ag	570	1060	72.0	60.9	55.6	23.8
Au	640	1180	5	0.7	0.36	0.049
B	660	1220	0.022	0.054	<0.001	<0.002
Be	645	1190	0.87	2.56	0.063	0.188
Bi	660(b)	1220(b)	3.4	0.45	<0.1	<0.01
Ca	620	1150	7.6	5.25	<0.1	<0.05
Cd	650(b)	1200(b)	6.7	1.69	0.47	0.11
Co	660	1220	1.0	0.46	<0.02	<0.01
Cr	660(c)	1220(c)	0.41	0.21	0.77	0.40
Cu	550	1020	33.15	17.39	5.67	2.48
Fe	655	1210	1.87	0.91	0.052	0.025
Ga	30	80	98.9	97.2	20.0	8.82
Gd	640	1180	11.5	2.18	<0.1	<0.01
Ge	425	800	53.0	29.5	6.0	2.30
Hf	660(c)	1220(c)	0.49	0.074	1.22	0.186
In	640	1180	17.5	4.65	0.17	0.04
Li	600	1110	9.9	30.0	4.0	13.9
Mg	450	840	35.0	37.34	14.9	16.26
Mn	660	1220	1.95	0.97	1.82	0.90
Mo	660(c)	1220(c)	0.1	0.03	0.25	0.056
Na	660(b)	1220(b)	0.18	0.21	<0.003	<0.003
Nb	660(c)	1220(c)	0.01	0.003	0.22	0.064
Ni	640	1180	6.12	2.91	0.05	0.023
Pb	660	1220	1.52	0.20	0.15	0.02
Pd	615	1140	24.2	7.5	<0.1	<0.02
Rh	660	1220	1.09	0.29	<0.1	<0.02
Ru	660	1220	0.69	0.185	<0.1	<0.02
Sb	660	1220	1.1	0.25	<0.1	<0.02
Sc	660	1220	0.52	0.31	0.38	0.23
Si	580	1080	12.6	12.16	1.65	1.59
Sn	230	450	99.5	97.83	<0.01	<0.002
Sr	655	1210	...	...	...	...
Th	635	1180	25.0	3.73	<0.1	<0.01
Ti	665(c)	1230(c)	0.15	0.084	1.00	0.57
Tm	645	1190	10.0	1.74	<0.1	<0.01
U	640	1180	13.0	1.67	<0.1	<0.01
V	665(c)	1230(c)	0.25	0.133	0.6	0.32
Y	645	1190	7.7	2.47	<0.1	<0.03
Zn	380	720	95.0	88.7	82.8	66.4
Zr	660(c)	1220(c)	0.11	0.033	0.28	0.085

(a) Eutectic reactions unless designated otherwise. (b) Monotectic reaction. (c) Peritectic reaction.

Liquid Solubility. Except for the partly miscible elements previously mentioned, all other metallic elements are completely miscible with aluminum in the liquid state. The solubility limits for a number of elements at temperatures above the melting point of aluminum are listed in Table 1. Of the semimetallic and nonmetallic elements, silicon is completely miscible with aluminum in the liquid state. Boron has a low solubility of about 0.02% at a eutectic temperature slightly below the melting point of aluminum. Its solubility increases with increasing temperature, but appears to be less than 1.5% at 1500 °C (2730 °F). Carbon has slight solubility in liquid aluminum; its solubility limits have not been completely established, but are indicated to be appreciably less than for boron.

Phosphorous and arsenic are nearly insoluble in aluminum. In hypothetical diagrams, sulfur has been indicated as having appreciable solubility in liquid aluminum. Early investigations indicated complete miscibility of selenium and tellurium with liquid aluminum. Although compounds are readily formed with aluminum, retention of more than trace amounts of these elements in the metal when melting and alloying are done under the usual atmospheric conditions is not possible. Three factors contribute to the difficulty of maintaining the composition: (1) high volatility of these elements at temperatures of liquid aluminum, (2) oxidation at the metal surface, and (3) formation of less dense compounds that separate to surface dross.

Except for hydrogen, common elemental gases and elements of the halogen group exhibit no detectable liquid solubility, but readily form compounds with aluminum. The solubility of hydrogen in both liquid and solid aluminum is discussed in Chapter 1 of this Volume. Figure 1 (Ref 1) shows the solubility of hydrogen in aluminum from 500 to 800 °C (930 to 1470 °F).

Solid Solubility. No element is known to have complete miscibility with aluminum in the solid state. Of all elements, zinc has the greatest solid solubility in aluminum (a maximum of 66.4 at.%). In addition to zinc, silver, magnesium, and lithium have solid solubilities greater than 10 at.% (in order of decreasing maximum solubility). Gallium, germanium, copper, and silicon (in decreasing order) have maximum solubilities of less than 10 but greater than 1 at.%. All other elements are less soluble. Solid solution limits for some elements in aluminum are recorded in Table 2.

The solid solution limits given for lithium are from recent investigations by Costa and Marshall (Ref 2) and by Levine and Rapperport (Ref 3). While the results of these investigators are in agreement, they differ considerably at temperatures below 500 °C (930 °F) from the results recently obtained by other investigators. Jones and Das (Ref 4) reported solubility limits of 4.2, 1.7, and 0.4% lithium, respectively, at the eutectic temperatures of 400 °C (750 °F) and 200 °C (390 °F).

With one known exception,* maximum solid solubility in aluminum alloys occurs at the eutectic, peritectic, or monotectic temperature. With decreasing temperature, the solubility limits decrease. This decrease from appreciable concentrations at elevated temperatures to relatively low concentrations at low temperatures is one fundamental characteristic that provides the basis for substantially increasing the hardness and strength of aluminum alloys by solution heat treatment and subsequent precipitation aging operations.

Intermetallic Phases. A feature of aluminum alloy systems is the wide variety of intermetallic phases, which occur because aluminum is highly electronegative and trivalent. The complete literature on intermetallic phases has been reviewed by Pearson (Ref 5). Intermetallic phases in aluminum alloy systems have also been discussed as part of a wider review by Mon-

*Tin shows a retrograde solid solubility between the melting point of aluminum and the eutectic temperature, 228.3 °C (442.9 °F), with a maximum of 0.10% at approximately 600 °C (1110 °F).

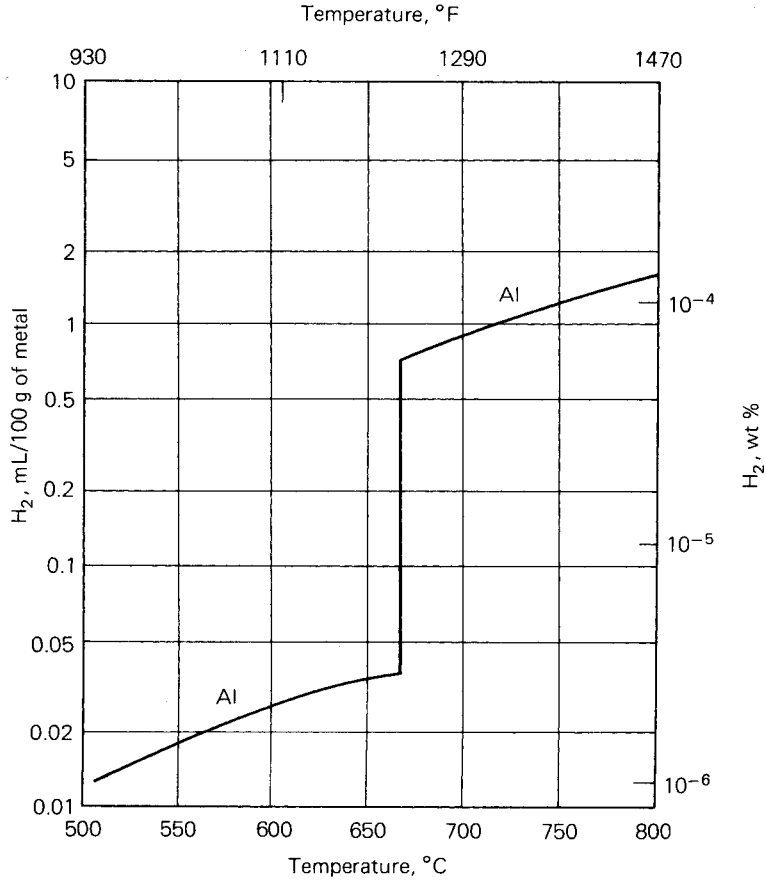

Fig. 1. Solubility of hydrogen at atmospheric pressure in aluminum and magnesium (Ref 1).

dolfo (Ref 6). The stability of such phases and the narrowness of their compositional range is determined by size and valency factors. In binary systems, some phases can be exactly stoichiometric, for example, AlSb. Other systems can have a very narrow compositional range not containing the composition of their formula, for example $CuAl_2$, thus containing lattice defects. Others such as Ag_2Al show wider compositional range. Transition metals often exhibit a succession with well defined and sometimes complex stoichiometry (Co_2Al_9, Co_4Al_{13}, $CoAl_3$, Co_2Al_5, and CoAl; and $MnAl_6$, $MnAl_4$, and $MnAl_3$). Transition metals also exhibit frequent metastability, in which one phase introduced during fast solidification transforms in the solid state to another, for example, $FeAl_6 \rightarrow FeAl_3$, or a metastable variant precipitates from supersaturated solid solution such as $MnAl_{12}$.

In ternary alloys, a few intermetallic phases of other binary systems can form a pseudobinary eutectic with primary aluminum solid solution, for example, Mg_2Si or $MgZn_2$. In quaternary systems, intermetallic phases

of the respective binary and ternary systems are occasionally isomorphous, forming continuous series of solid solutions in equilibrium with aluminum solid solution. An important example is in the aluminum-copper-magnesium-zinc quaternary system, where there are three such pairs: $CuMg_4Al_6$ + $Mg_3Zn_3Al_2$, Mg_2Zn_{11} + $Cu_6Mg_2Al_5$, and $MgZn_2$ + CuMgAl. The first pair have similar lattice parameters and form extensive mutual solid solution, the others less so. Neither $Cu_6Mg_2Al_5$ nor CuMgAl are equilibrium phases in aluminum-copper-magnesium, although both Mg_2Zn_{11} and $MgZn_2$ are equilibrium phases in aluminum-magnesium-zinc.

Table 2. Solid Solution Characteristics of Binary Aluminum Alloys

Element	ΔH_s(a) kJ/g-atom	μΩ/at.%(b)	$\Delta a/\Delta_Y$(c) m/at.% × 10^{10}	$\gamma_Y - \gamma_{Al}$(d) m × 10^{10}
Ag	26.7	1.15	Nil	+0.013
Au	87.5	2	...	+0.010
B	...	...	...	−0.449
Be	75.7	0.085	−0.0217	−0.306
Bi	...	...	...	+0.347
Ca	...	...	...	+0.541
Cd	82.0	0.057	−0.0067	+0.079
Co	...	...	...	−0.177
Cr	67.8	7.70	−0.0100	−0.153
Cu	41.0	0.785	−0.0051	−0.153
Fe	95.8	4.75	...	−0.169
Ga	19.2	0.250	+0.0012	−0.025
Gd	...	...	...	+0.375
Ge	40.6	0.775	+0.00155	+0.015
Hf	(77.8)	...	...	+0.156
In	...	...	...	+0.150
Li	26.8	0.89	−0.00016	+0.120
Mg	18.8	0.49	+0.00460	+0.169
Mn	60.7	5.97	−0.0066	−0.161
Mo	...	8.35	...	−0.043
Na	...	...	...	+0.467
Nb	...	6.85	...	+0.027
Ni	95.8	1.77	...	−0.185
Pb	...	1.5	...	+0.275
Pd	51.0	2.35	...	−0.056
Rh	...	...	...	−0.077
Ru	...	...	...	−0.093
Sb	...	...	...	+0.228
Sc	69.5	3.32	...	+0.191
Si	49.4	0.65	−0.0018	−0.054
Sn	...	1.1	...	+0.194
Sr	...	3.2	...	+0.719
Th	...	...	...	+0.366
Ti	64.0	5.10	−0.0105	+0.038
Tm	...	...	...	+0.330
U	...	...	...	+0.087
V	73.6	6.90	−0.0075	−0.091
Y	...	...	...	+0.368
Zn	8.5	0.211	−0.00075	−0.090
Zr	86.2	5.85	...	+0.168

(a) Heat of solution from slope of line for ln solubility versus 1/T (for dilute solutions for elements silver and zinc). (b) Increase in electrical resistivity per 1 at.% in solid solution. (c) Change in aluminum lattice parameter per 1 at.% in solid solution. (d) Difference between Pauling metallic radii of element and aluminum.

Table 3. Intermetallic Phases in Aluminum-Rich Aluminum Alloy Systems

Intermetallic phase	ASTM E157-61T designation	Other designation	Structure type		Space group	Lattice parameter, A		
						a	b	c
Binary Systems								
Ag_2Al	(Ag,Al)2*H*	ζ	A_3	Hex	$P6_3/mmc$	2.885	...	4.582
αAlB_{12}	(B,Al)52*N*	...	...	Mono	$C2/m$	8.522	11.002	7.393
βAlB_{12}	(B,Al)208*T*	...	...	Tet	...	12.58	...	10.20
AlB_2	(B,Al)3c*H*	...	C32	Hex	...	3.006	...	3.252
$CaAl_4$	(Al,Ca)10*U*	...	$D1_3$	bc Tet	$I4/mmm$	4.362	...	11.09
Co_2Al_9	(Al,Co)22*M*	...	...	Mono	$P2_1/c$	6.213	6.290	8.556
$CrAl_7$	...	...	...	Ortho	...	24.8	24.7	30.2
$Cr \cdot Al_{11}$	...	...	...	Ortho	...	24.8	24.7	30.2
$CuAl_2$	(Al,Cu)12a*U*	θ	C16	bc Tet	$I4/mcm$	6.066	...	4.874
		θ′	...	Tet	...	4.04	...	5.80
		GP[2] or θ″	...	Tet	...	4.04	...	7.68
$FeAl_4$	...	...	...	Mono	$C2/m$	15.520	8.099	12.501
$FeAl_6$	...	...	...	Ortho	$CCmm$	6.464	7.440	7.779
AlLi	(Al,Li)16*F*	...	B32	bcC	$Fd3m$	6.38	...	...
Mg_2Al_3	(Al,Mg)1166*F*	β	...	fcC	$Fd3m$	28.16	...	...
$MnAl_6$	(Al,Mn)28*Q*	...	...	Ortho	$Cmcm$	6.498	7.552	8.870
$MnAl_4$	...	...	...	Hex	...	28.41	...	12.38
$MnAl_{12}$	...	G	...	Cubic	...	~7.47	...	...
$NiAl_3$	(Al,Ni)16c*O*	ϵ	$D0_{20}$	Ortho	$Pnma$	6.611	7.366	4.812
Ni_2Al_3	(Al,Ni)5b*H*	δ	$D5_{13}$	Hex	$P3m1$	4.036	...	4.900
NiAl	(Ni,Al)2*B*	β	B2	bcC	$Pm3m$	2.887	...	...
AlSb	(Al,Sb)8*F*	...	B3	Cubic	$F43m$	6.096	...	...
$TiAl_3$	(Al,Ti)8*U*	...	$D0_{22}$	bc Tet	$I4/mmm$	3.848	...	8.596
UAl_4	(Al,U)20*P*	...	$D1_b$	bc Ortho	$Imma$	4.41	6.27	13.71
VAl_{11}	(Al,V)192*F*	...	...	fcC	$Fd3$	14.586	...	...
VAl_6	(Al,V)56*H*	...	...	Hex	...	7.718	...	17.15
$ZrAl_4$	(Al,Zr)16c*U*	...	$D0_{23}$	bc Tet	$I4/mmm$	4.013	...	17.320
TiB_2	(B,Ti)3*H*	...	C32	Hex	$P6/mmm$	3.028	...	3.228
Mg_2Si	(Mg,Si)12*F*	β	C1	fcC	$Fm3m$	6.351	...	...
		β′	...	Hex	...	7.05	...	4.05/12.15
Mg_2Zn_{11}	(Zn,Mg)39*C*	Z	...	Cubic	$Pm3$	8.552	...	...
$MgZn_2$	(Zn,Mg)12*H*	M	C14	Hex	$P6_3/mmc$	5.18	...	8.517
Ternary Systems								
$Cr_2Mg_3Al_1$	(Al,Mg,Cr)184*F*	E	...	fcC	$Fd3m$	14.55	...	...
$(Cr,Mn)Al_{12}$	(Al,Mn,Cr)26*B*	G	...	bcC	$Im3$	7.507	...	...
$Cr_4Si_4Al_{13}$	(Al,Cr,Si)84*F*	α	...	fcC	$F43m$	10.917	...	...
Cu_2FeAl_7	(Al,Cu,Fe)40*T*	β or N	...	Tet	$P4/mnc$	6.336	...	14.870
$(Fe,Cu)(Al,Cu)_6$	(Al,Fe,Cu)28*Q*	α	...	Ortho	$Cmcm$	7.464	6.441	8.786
$Cu_5Li_2Al_{15}$	...	T_B	C1	fcC	$Fm3m$	5.83	...	...
$CuLiAl_2$	...	T_1	...	Hex	...	4.96	...	9.35
$CuLi_3Al_6$	...	T_2	...	...	...	...	...	...
$CuMgAl_2$	(Al,Cu,Mg)16*S*	S	...	fc Ortho	$Cmcm$	4.01	9.25	7.15
CuMgAl	(Al,Cu,Mg)12*H*	U or M	C14	Hex	$P6_3/mmc$	5.07	...	8.29
$CuMg_4Al_6$	(Al,Mg,Cu)162*B*	T	...	bcC	...	14.31	...	...
$Cu_3Mg_6Al_7$	(Al,Mg,Cu)96*B*	Q or Y	...	Cubic	$Im3$	12.087	...	...
$Cu_6Mg_2Al_5$	(Cu,Al,Mg)39*C*	V or Z	...	Cubic	$Pm3$	8.311	...	...
$Cu_2Mn_3Al_{20}$	...	T	...	Ortho	...	24.11	12.51	7.71
Cu_3NiAl_6	(Al,Cu,Ni)250*B*	T	...	bcC	...	14.6	...	...
Cu_3ZnAl_3	...	T′	...	bcC	...	2.911	...	...
$FeNiAl_9$	...	...	...	Mono	...	...	...	...
Fe_2SiAl_8	...	αFeSi	...	Hex	$P6_3/mnc$	12.3	...	26.3
	$(FeM)_3Si_2Al_{15}$	α′FeSi		bcC	$Im3$	12.548	...	...
$FeSiAl_5$	...	βFeSi	...	Mono	...	6.12	6.12	41.48
$FeSi_2Al_4$	...	δFeSi	...	Tet	...	6.16	...	9.49
Mg_2MnAl_{10}	...	T	...	...	...	...	...	...
$Mg_3Zn_3Al_2$	(Mg,Zn,Al)162*B*	T	...	bcC	$Im3$	14.19	...	...
$Mn_3Si_2Al_{15}$	...	αMnSi	...	Cubic	...	12.652	...	...
Mn_3SiAl_{10}	(Al,Mn,Si)26*H*	βMnSi	...	Hex	$P6_3/mmc$	7.513	...	7.745
Quaternary Systems								
$Cu_2Mg_8Si_6Al_5$	...	...	...	Hex	...	10.32	...	4.05
$CuMg_5Si_4Al_4$	...	...	...	bcC	...	12.63	...	...
$FeMg_3Si_6Al_8$	(Al,Si,Mg,Fe)18c*H*	...	...	Hex	$P62m$	6.63	...	7.94

(a) Peritectic decomposition.

c/a, α or β	Atoms per unit cell	Density: Measured g/cm³	Density: Measured lb/in.³	Density: Calculated g/cm³	Density: Calculated lb/in.³	Melting temperature °C	Melting temperature °F
1.588	2	...	...	8.14	2.94	730(a)	1350(a)
143° 29′	52	...	...	2.53	0.913	...	...
0.811	208	...	...	2.58	0.931	~1350	~2460
1.082	3	...	...	3.17	1.14	~850(a)	~1560(a)
2.542	10	...	...	2.33	0.841	700(a)	1290(a)
94° 46′	22	3.60	1.30	3.60	1.30	1940(a)	1720(a)
...	1160	...	...	3.14	1.13	~725(a)	~1340(a)
...	1209	...	...	3.34	1.21	~940(a)	~1720(a)
0.803	12	4.34	1.57	4.35	1.57	590	1090
1.436	6	...	...	4.12	1.49	...	...
1.901	8	...	...	3.83	1.38	...	...
107° 43′	~100	3.77	1.36	3.78	1.36	1160(a)	2120(a)
...	42	3.45	1.25	3.45	1.25	...	...
...	16	...	...	1.725	0.6232	717	1322
...	1166	2.23	0.805	2.23	0.805	450	840
...	28	3.27	1.18	3.31	1.19	710(a)	1310(a)
0.436	...	...	...	...	...	820(a)	1510(a)
...	...	...	...	...	...	...	...
...	16	...	...	3.96	1.43	855(a)	1570(a)
1.214	5	...	...	4.76	1.72	1130(a)	2070(a)
...	2	...	...	5.91	2.13	1640	2980
...	8	4.34	1.57	...	...	~1050	~1920
2.234	8	3.31	1.19	3.37	1.22	1340(a)	2440(a)
...	20	...	...	6.06	2.19	730(a)	1350(a)
...	192	...	...	2.98	1.08	670(a)	1240(a)
2.222	56	...	...	3.20	1.16	740(a)	1360(a)
4.316	16	4.11	1.48	4.11	1.48	1580	2880
1.064	3	4.38	1.58	4.50	1.62	2790	5050
...	12	...	...	1.99	0.718	1100	2010
...	...	...	...	...	...	...	...
...	39	6.16	2.22	6.12	2.21	385(a)	725(a)
1.644	12	5.20	1.88	5.20	1.88	590	1090
...	184	2.80	1.01	2.86	1.03	...	...
...	26	...	...	2.92	1.05	<580	<1080
...	84	3.40	1.23	...	...	...	...
2.347	40	4.30	1.55	4.44	1.60	...	...
...	28	...	...	...	...	630(a)	1170(a)
...	...	...	...	...	...	...	...
1.885	...	...	...	...	...	...	...
...	...	...	...	...	...	...	...
...	16	...	...	3.55	1.28	~550(a)	~1020(a)
1.64	12	...	...	4.13	1.49	~950	~1740
...	162	...	...	2.69	0.971	~475(a)	~890(a)
...	96	3.02	1.09	...	...	~520(a)	~970(a)
...	39	4.94	1.78	4.90	1.77	~710(a)	~1310(a)
...	150	...	...	3.59	1.30	...	...
...	250	...	...	5.48	1.98	~820(a)	~1510(a)
...	...	...	...	...	...	...	...
...	...	...	...	...	...	~810(a)	~1490(a)
...	...	3.58	1.29	...	...	~860(a)	~1580(a)
...		...	...	...	...	...	...
91°	...	...	...	...	...	~700(a)	~1290(a)
1.54	...	3.00	1.08	...	...	~870(a)	~1600(a)
...	...	...	...	...	...	...	...
...	162	3.78	1.36	3.80	1.37	~530(a)	~990(a)
...	...	...	...	...	...	...	...
1.031	~26	3.74	1.35	...	...	...	...
0.392	...	2.79	1.01	...	...	...	...
...	...	...	...	...	...	...	...
1.20	18	2.82	1.02	2.82	1.02	...	...

Another instance is in the aluminum-iron-manganese-silicon quaternary system; here the stable phase $(FeMn)_3Si_2Al_{15}$ (body-centered cubic) can vary from $Mn_3Si_2Al_{15}$, a = 1.2652 nm (12.652 Å) to $\sim(Mn_{0.1}Fe_{0.9})_3Si_2Al_{15}$, a = 1.2548 nm (12.548 Å). The stable phase of the closest composition in aluminum-iron-silicon is Fe_2SiAl_8 (hexagonal); the hexagonal → cubic transition is also accomplished by small additions of vanadium, chromium, molybdenum, and tungsten, and larger additions of copper (Ref 7). Such chemical stabilization effects, coupled with the metastability introduced by casting, frequently cause complex alloy structure.

The origin of this vast range of structures has been the subject of considerable study (Ref 8). Some phases are normal valency compounds (ionic), with high melting points and low electrical conductivity, such as Al-Group V compounds like AlSb. For these, electron transfer occurs, and bonding is nondirectional; interionic spacing is less than is expected for metallic bond. Some phases are electron compounds with specific valency electron/atom ratios, for example, 3-to-2 for $AlCu_3$. No electron transfer occurs in this phase, and factors relating to the metallic bond predominate. These compounds have some ductility, reasonable electrical conductivity, and melting points that range between those of the alloying components.

The origin of aluminum-transition metal and silicon-phases is still being investigated. There is some evidence that the valency electrons are absorbed into the d-shell of the transition metals and are replaced by electrons from the aluminum shell. This leads to a reduction of some aluminum-transition metal spacings as for the ionic bond; these phases have high melting points. Some systemization has been attempted (Ref 9). The structures can be considered in terms of flattened, polyhedral groupings of aluminum atoms around the transition metal atoms, 8-, 9-, or 10-fold. The three-dimensional structures are controlled by the packing of these polyhedra. Crystal structures, lattice parameters, and density and melting point or peritectic decomposition temperature for the most important intermetallic phases of aluminum-rich alloys are given in Table 3.

EQUILIBRIUM AND NONEQUILIBRIUM SOLIDIFICATION

All commercial solidification processes involve some nonequilibrium effects. Although equilibrium solidification is not actually observed, it is of interest as a limiting case. In real casting processes, the extent of deviation from equilibrium conditions has a significant effect on the actual microstructure observed (Ref 10 and 11).

Equilibrium solidification is approached when $L^2 \ll D_s t$, where L is the length solidified, D_s is the diffusion coefficient of solute in the solid, and t is time. This situation is illustrated in Fig. 2. An alloy of overall composition, C_0, begins to freeze at T_L and is frozen at T_S. The initial solid to freeze has a solute concentration given by kC_0, where k is the equilibrium partition coefficient (C_S^*/C_L^*), the ratio of interfacial solid and liquid solute concentrations. Because diffusion in the solid is assumed to be complete, the bulk solid solute concentration (C_S) is equal to the interfacial solid solute concentration (C_S^*) on the solidus line. Diffusion

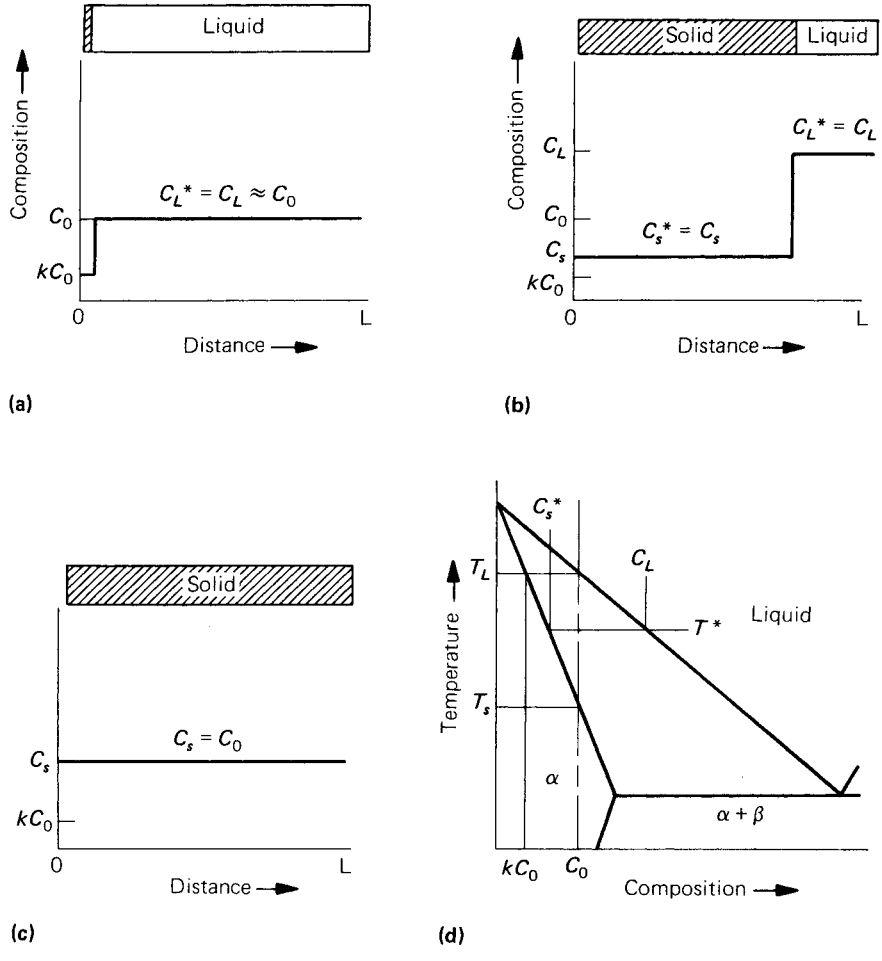

Fig. 2. Solute redistribution in equilibrium solidification of an alloy of composition C_0: (a) at start of solidification; (b) at temperature T; (c) after solidification; and (d) phase diagram (Ref 10).*

in the liquid is also assumed to be complete. After freezing, a uniform, single-phase solid with a solute concentration of C_0 is obtained.

Solidification with Local Equilibrium. Many commercial solidification processes, operating at moderate cooling rates (0.1 to 100 °C/s or 0.18 to 180 °F/s) can be approximated by the assumption that $D_S \simeq 0$ and local equilibrium at the interface is maintained ($k = C_S^*/C_L^*$) and $D_L \simeq \infty$. Solidification under these conditions is illustrated in Fig. 3. The first solid to freeze, at T_L, has a solute concentration of kC_0. At temperatures below the liquidus, the solid forming at the freezing interface is higher in solute than that previously frozen. To maintain a solute balance, additional solute is present in the liquid as a consequence of coring. This results in the formation of nonequilibrium eutectic in interdendritic re-

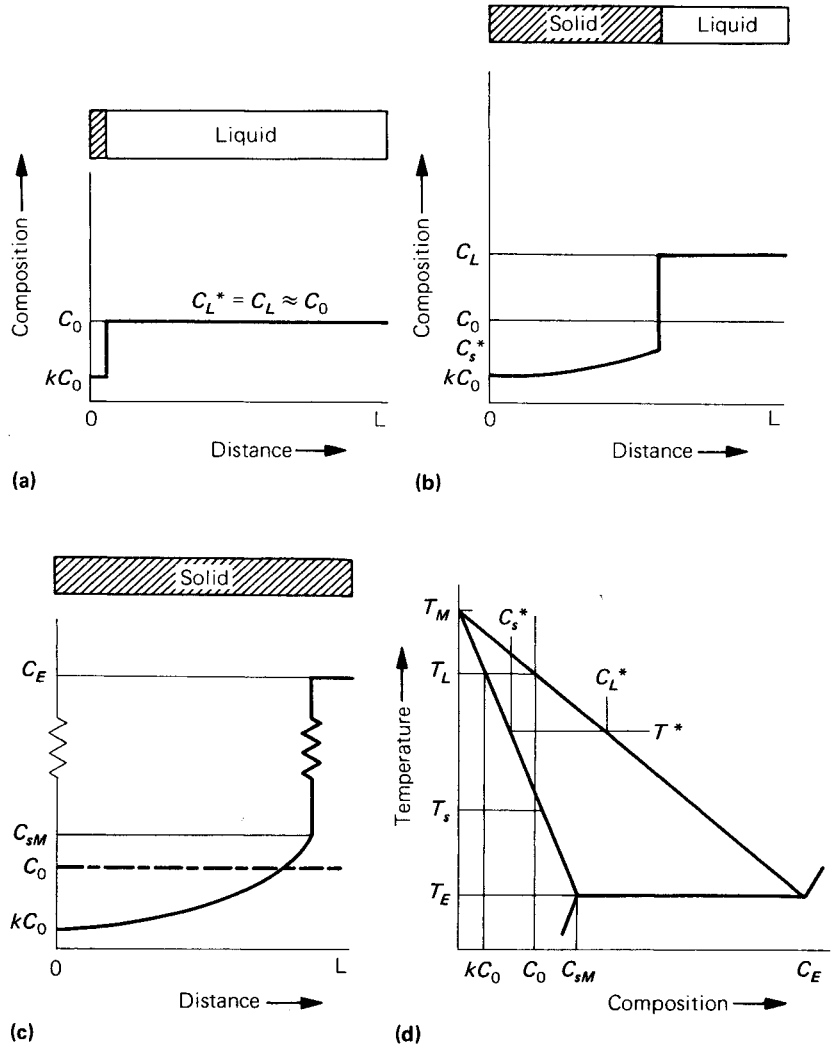

Fig. 3. Solute redistribution in solidification with no solid diffusion and complete diffusion in the liquid: (a) at start of solidification; (b) at temperature T; (c) after solidification; and (d) phase diagram (Ref 10).*

gions at the end of freezing. The amount of eutectic formed is to be given by:

$$f_E = \left(\frac{C_E}{C_0}\right)^{1/(k-1)} \qquad \text{(Eq 1)}$$

where f_E is the volume fraction eutectic and C_E is the eutectic solute concentration. The amount of eutectic actually observed is close to that predicted by Eq 1 for the cooling rate in the range of typical ingot casting processes (Ref 12). The dissolution of this nonequilibrium eutectic is achieved during ingot homogenization (Ref 13).

Rapid Solidification of Aluminum Alloys. In the search for improved properties for aluminum alloys, a variety of techniques that involve direct quenching from the liquid state have been investigated. These techniques, referred to as rapid solidification processing (RSP), are aimed at achieving a highly efficient dissipation of heat away from the liquid-solid interface so that a substantial increase in undercooling and the corresponding interface velocity can be obtained. This objective usually implies an improved heat transfer coefficient at the casting-quenchant surface and an increase in the surface area-to-volume ratio of the casting. The overall effect is the achievement of cooling rates estimated at from 10^3 to 10^{10} °C/s (1.8×10^3 to 1.8×10^{10} °F/s). A second guideline in RSP is to obtain a sufficient degree of supercooling before nucleation so that the liquid acts as the main sink for the heat of fusion. The solidification then proceeds in an essentially adiabatic manner. Solidification under the increasingly higher cooling rates, and conceivably, higher undercoolings typical of atomization, splat cooling, and other related techniques, usually results in progressive departure from the regular microstructures produced by conventional casting.

Microstructures of Rapidly Solidified Aluminum Alloys

Rapid solidification of aluminum alloys usually results in one or more of the following microstructural modifications:

- Microstructural refinement manifested as smaller grain size, as well as smaller dendrite arm and eutectic spacings
- Extension in terminal solid solubility of alloying elements in the primary α-aluminum phase and change in segregation patterns eventually leading to the reduction or elimination of the second phase
- Morphological changes of the eutectic or the primary phase
- Formation of metastable phases
- Coupled eutectic growth at off-eutectic compositions
- Vacancy supersaturation

Although all these effects have been observed in aluminum alloys, some even at the moderate cooling rates of 10 to 10^3 °C/s (18 to 1.8×10^3 °F/s) only the first four, which are important in terms of improving the properties of the final product, are well understood. A discussion of these effects follows.

Microstructural Refinement. In general, the fineness of microstructure during dendritic solidification of aluminum alloys, as in most other alloy systems, can be correlated to the average cooling rate during solidification, ϵ_{Avg}, or local solidification time (time available for coarsening), t_f, by:

$$DAS = a\epsilon_{Avg}^{-m} = bt_f^m \qquad \text{(Eq 2)}$$

and

$$\epsilon_{Avg} = \frac{(T_L - T_S)}{t_f} \qquad \text{(Eq 3)}$$

where $(T_L - T_S)$ is the solidification temperature range, DAS is the dendrite arm spacing, and a, b, and m are constants.

Experimental relationships between average cooling rate and dendrite arm spacing are available for several aluminum alloys (Ref 14 and 15). For example, dendrite arm spacings for an Al-10.5% Si alloy versus average cooling rates are reported for cooling rates of up to 10^5 °C/s (1.8×10^5 °F/s) (Ref 16). Dendritic spacings of 0.01 to 0.5 μm (0.0004 to 0.02 mil) (Ref 17–20), and eutectic spacings in the same order of magnitude (Ref 21), have been reported for electron-transparent areas of aluminum alloy gun splats on copper substrates. However, in most studies, experimental difficulties have limited the range of accurately measured cooling rates to less than ~10^3 °C/s (~1.8×10^3 °F/s).

Figure 4 illustrates the capabilities of various solidification techniques in terms of microstructural refinement expected from the estimated achievable cooling rates and a relationship of the type given by Eq 2 for aluminum alloys. Caution must be exercised when the exponential correlation in Eq 2 is used to estimate cooling rates in RSP from the dendrite spacings, because the reliability of extrapolating this relationship over many orders of magnitude is probably poor, especially if the microstructures examined do not exhibit typical dendritic morphologies. Furthermore, the constants in Eq 2 vary with alloy composition. Studies on the effect of alloy composition on structure at a fixed average cooling rate for aluminum binary alloys with copper, magnesium, silicon, or zinc have shown that increasing the solute content refines the dendrite arm spacing, especially at low solute concentrations (Ref 15 and 23). Refinement of secondary phases, including eutectic constituents, also occurs with an increasing cooling rate during solidification. Dispersion hardening associated with this effect has been reported in aluminum-silicon-based alloys (Ref 24–27).

Rapid solidification processing can also produce grain sizes of ~1 μm (~0.04 mil), significantly smaller than those developed in conventional casting. A quantitative analysis of the grain refinement resulting from solidification at high cooling rates (>10^5 °C/s or >1.8×10^5 °F/s) obtained by splat quenching has been made by Boswell and Chadwick (Ref 28), and good agreement was obtained between observed and predicted grain sizes for rapidly quenched aluminum.

Extension in Solid Solubility. Terminal solid solubility extension has been obtained at sufficiently high cooling rates in almost all aluminum alloy systems investigated, with the notable exception of aluminum-zinc (Ref 29). The increased solid solubility permits higher alloying levels, resulting in superior strength-ductility combinations in a number of systems. Table 4 shows the maximum reported solid solubilities for a number of binary aluminum alloys of practical interest.

There are indications that the extent of solute solubility increases with severity of the quench (Ref 30) and increased initial alloy composition (Ref 31) and that it is not necessarily bounded by the eutectic composition. Additions especially susceptible to solubility extension in binary alloys (for example, manganese) can be used in ternaries to increase the solubility limit of less susceptible elements such as iron, cobalt, and nickel (Ref 30).

Morphological Modifications. Both conventional dendritic (columnar and equiaxed) and modified dendritic morphologies have been reported

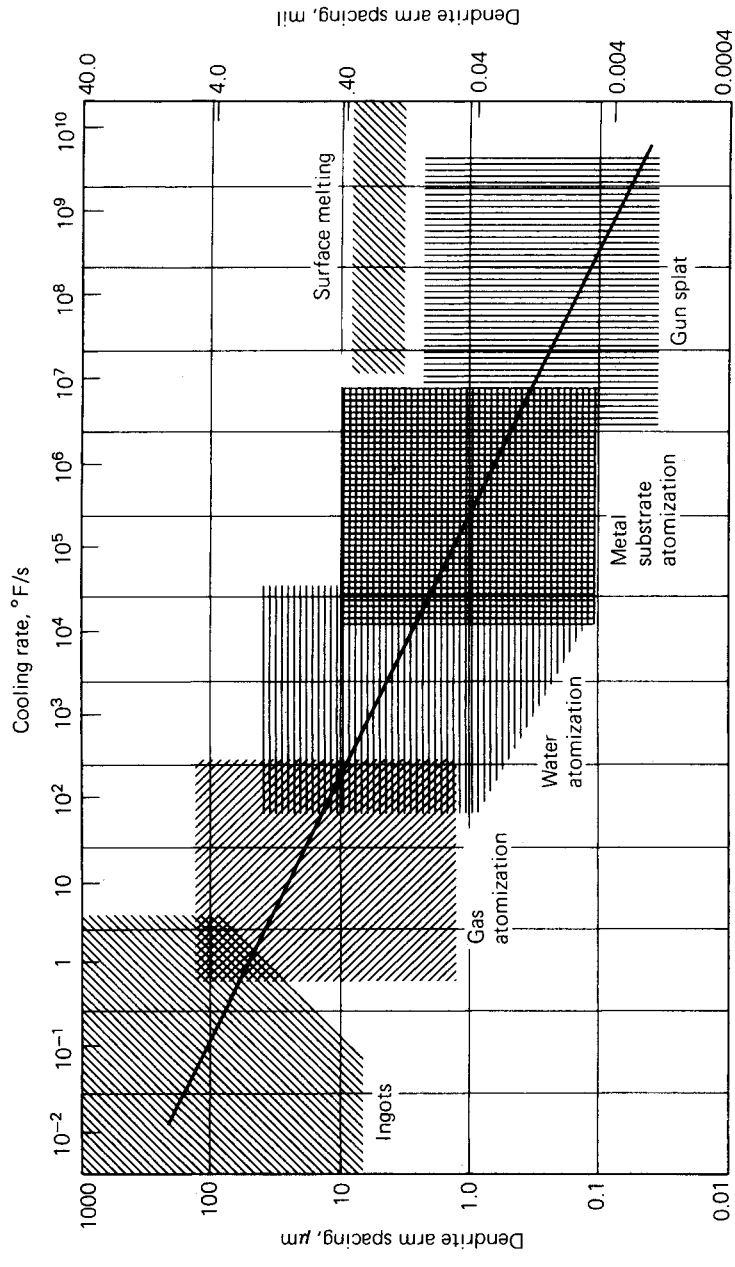

Fig. 4. Dendrite arm spacing as a function of cooling rate for aluminum and aluminum alloys (Ref 22).

Table 4. Extension of Solid Solubility in Binary Aluminum Alloys Quenched from the Melt

Element	Maximum at equilibrium Temperature at.%	K	°R	Reported maximum, at.%
Cr	0.44	935	1670	>5–6
Cu	2.5	820	1460	17–18
Fe	0.025	930	1660	4–6
Mg	18.9	725	1290	36.8–40
Mn	0.7	925	1650	>6–9
Ni	0.023	915	1600	1.2–7.7
Si	1.59	850	1520	10–16
Zn	66.5	655	1170	38–···

Source: H. Jones, *Aluminum*, Vol 54 (No. 4), 1978, p 274.

in alloys solidified at high cooling rates (Ref 32–34). The primary phase in the latter tends to assume a cellular or rod-like configuration with progressively faster cooling rates (Ref 18 and 34). Similar observations have been reported in bulk specimens of nickel- and iron-based alloys with increasing supercooling before nucleation of the solid phase (Ref 35). High cooling rates sometimes can suppress primary formation of an equilibrium phase from the melt. For example, formation of α-aluminum dendrites instead of equilibrium $FeAl_3$ phase in hypereutectic aluminum-iron alloys both in chill-cast (Ref 36) and splat-cooled specimens (Ref 37) has been reported.

Sufficiently rapid cooling rates during solidification can alter the composition range of cooperative eutectic growth, the eutectic constituents, and their morphologies. Relatively rapid solidification of aluminum-iron alloys in the range of 10 to 10^4 °C/s (18 to 1.8×10^4 °F/s) has resulted in eutectic morphologies changing from irregular Al—$FeAl_3$ to regular Al—$FeAl_6$, as well as coupled eutectic growth at noneutectic compositions (Ref 36). In addition, degenerate and radial eutectic structures in Al-17.3 at.% Cu and structural changes as a function of copper content have been studied via splat cooling (Ref 38).

Formation of Metastable Phases. Departure from the phase equilibria predicted by the phase diagram of aluminum alloys is not as common as the effects noted above. Nevertheless, a certain number of cases are reported in the literature and have been classified by Jones (Ref 30) as:

- Type I: phases present at equilibrium but not stable at the temperature and alloy compositions in which they were observed
- Type II: phases not formed from the melt but appearing, normally transiently, on further heat treatment or precipitated during quenching through the solid state
- Type III: phases present in the rapidly quenched specimen but not known to exist under equilibrium conditions at any composition within the alloy system

A summary of the reported observations in binary aluminum alloy systems is given in Table 5. The only report of a noncrystalline structure in an aluminum alloy (Ref 39), splat-cooled Al-17.3 at.% Cu alloy, has not been supported by further investigation (Ref 40).

Table 5. Nonequilibrium Phases Detected in Aluminum Binary Alloys Under Rapid Solidification

Alloying element	Concentration range, at.%	Nonequilibrium phase detected	Type	Corresponding equilibrium phases	
Cr	1.6–3	Al_4Cr	I	α-Al + Al_7Cr(a)	(Ref 1)
Cu	45	Al_3Cu_2 (trigonal)	III	O + η_2	(Ref 2)
	17.3	Noncrystalline	III	α-Al + O(a)	(Ref 3)
Fe	2–4	γ, γ′, γ″, o^{α}	II	Al_3Fe + α-Al	(Ref 4)
	4	Al_6Fe (orthorhombic)	II	...	(Ref 4)
	...	Al_6Fe	III	...	(Ref 5)
Mg	25	Le_2 superlattice	II	α-Al + β-Al_3Mg_2(a)	(Ref 5)
	40	(α-Mn)-like structure	III	α-Al + β-Al_3Mg_2(a)	(Ref 5)
	(b)	...	...	...	...
Mn	≤6	Al_4Mn	I	α-Al + Al_6Mn(a)	(Ref 6)
Ni	7.3–10.1	η (orthorhombic)	III	α-Al + β-Al_3Ni(a)	(Ref 7)

(a) Formed transiently during aging following a decomposition kinetics similar to the supersaturated aluminum-copper solid solutions. (b) Concentration range, ~10 wt%.
(Ref 1) Varich and Lyukevich, 1970. (Ref 2) Ramachandrarao and Lavidjoni, 1974. (Ref 3) Davies and Hull, 1974. (Ref 4) Jacobs, *et al.*, 1974. (Ref 5) Jones, 1978. (Ref 6) Varich and Kolesnichenko, 1961. (Ref 7) Toneje, *et al.*, 1971

Particular nonequilibrium effects do not happen above a critical thickness in splat cooling (below a given average cooling rate during solidification). For example, $FeAl_6$ can displace the equilibrium phase $FeAl_6$ at cooling rates as low as 3 °C/s (5 °F/s); however, cooling rates of the order of 10^4 °C/s (1.8×10^4 °F/s) are required to displace the equilibrium FCC Al_3Mg_2 phase in aluminum-magnesium alloys (Ref 30).

PHASE DIAGRAMS AND THERMODYNAMICS

Aluminum is alloyed with a large number of elements. Commercial alloys frequently contain more than one second phase, with the overall properties achieved by careful control of second-phase type, shape, size, and distribution. Consequently, the generation and understanding of phase diagrams has played an important part in aluminum technology.

Phase diagrams map phase stability in terms of important variables, usually temperature and composition. They are determined by fundamental thermodynamic factors. This section identifies these factors and discusses how they can be used to systemize alloying behavior, interpolate or extrapolate data, or predict unknown phase diagrams. The analytical treatment is limited and based on more specialized texts (Ref 41–43).

Background. Thermodynamics is concerned with the energy involved in the transfer of material from one phase to another, with the same or different composition. It does not by itself determine structural features such as crystallography, subdivision of a second phase, or rate of transfer. At constant temperature, T, and pressure this energy is the change in the Gibbs free energy of the system (ΔG) and is comprised of two factors, the enthalpy change (ΔH) and entropy change (ΔS), as shown below:

$$\Delta G = \Delta H - T\Delta S \qquad \text{(Eq 4)}$$

For the process to be spontaneous, ΔG must be negative, and for equilibrium, ΔG must be zero. ΔH represents the heat evolved or absorbed

during the reaction, negative for an exothermic reaction, and is determined by changes in bond energies or lattice strain because of atomic size difference. ΔS is determined primarily by changes in vibrational frequency, as is seen from its dependence on the change of heat capacity:

$$\Delta S = \int_0^T \frac{\Delta C_p}{T} dT$$

For solution reactions, ΔS is usually positive because of the complexity of vibrational spectrum of a mixture of atoms. It is also positive on liquation because of the breakdown of crystalline order.

Quantitative assessment of phase boundary position is determined through the concept of chemical potential, μ. This is the free energy/mole of a component of a solution at equilibrium and is the same everywhere within a system of phases. It is defined with respect to the free energy/mole of the pure component in the same physical state, μ_0:

$$\mu = \mu_0 + RT \ln a \qquad \text{(Eq 5)}$$

where R is the gas constant and a is the activity. A solution is termed ideal if activity equals mole fraction, X (atom fraction for metallic solutions). Physically, this means that bond energies and atom sizes are identical for solute and solvent, giving zero enthalpy and volume change on mixing. Most aluminum-based solutions are far from ideal except at very low concentration. However, the ideal solution model does give insight into some important characteristics of phase diagrams.

Liquidus and Solidus. Liquidus and solidus represent the variation with temperature of composition of liquid and solid solutions in equilibrium. Thus, for any component, $\mu^S = \mu^L$. This must be translated into a more usable form. For ideal solutions, atom fractions can be substituted in Eq 5 and equate:

$$RT \ln \frac{X^L}{X^S} = \mu_0^S - \mu_0^L \qquad \text{(Eq 6)}$$

From the definition of μ_0, $-(\mu_0^S - \mu_0^L)$ is the molar free energy of fusion of the pure component at temperature T displaced from T_f, the equilibrium fusion temperature. Hence, it is nonzero. If the fusion enthalpy ΔH_f (the latent heat of fusion) is assumed to be independent of temperature and composition, Eq 4 at T and T_f can be used to give $\Delta G_{f,T} = \Delta H_f(T_f - T)/TT_f$. Therefore:

$$\ln \frac{X^L}{X^S} \cong \frac{\Delta H_f}{RT_f} - \frac{\Delta H_f}{RT} = \frac{\Delta S_f}{R} - \frac{\Delta H_f}{RT} \qquad \text{(Eq 7)}$$

This relationship can be tested in two ways. The first is to use data for eutectic and peritectic invariant points which are relatively easy to establish (Table 1). When $1/T$ is plotted against log $(X^L/X^S)_{Al}$, the results should be close to the ideal solution line with slope $-2.303\ R/\Delta H_{f,Al}$. This is shown in Fig. 5; the data correlate well. The second method is to use data for individual solidus and liquidus curves of systems with higher solubilities as shown in Fig. 6. That closest to the ideal case is aluminum-gallium; gallium has similar atomic radius (Table 2) and, being in the same group of the periodic table, the same outer electronic structure. The unusual behavior of aluminum-zinc is probably associated with clustering in the solid solution.

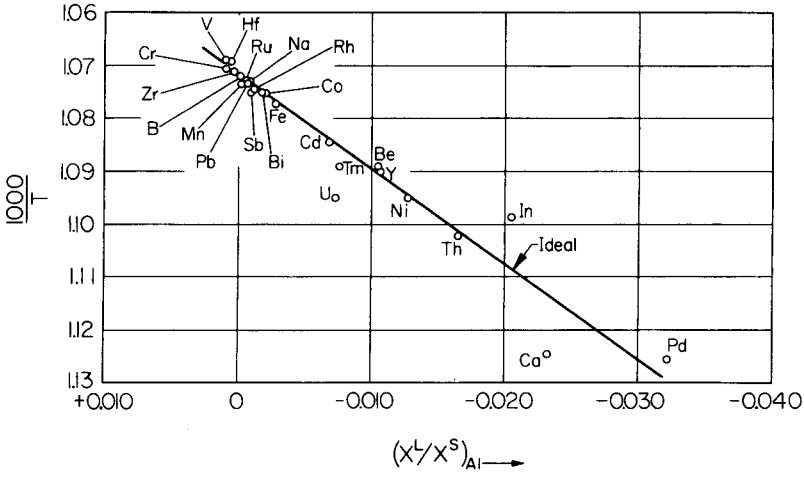

Fig. 5. Equilibrium eutectic and peritectic invariant point data for binary aluminum alloy systems plotted according to Eq 7 so as to show correlation with the ideal solution model (Ref 44).

The parameter that describes the heterogeneity of solute distribution in the primary phase after casting is the partition ratio, $k = (X^S/X^L)_{solute}$. When experimental values are not available, k can be calculated thermodynamically in two ways (Ref 42). For ideal aluminum + B solutions:

$$k = \exp\left[\frac{\Delta H_{f,B}(T_{f,Al} - T_{f,B})}{RT_{f,Al}T_{f,B}}\right] \qquad \text{(Eq 8)}$$

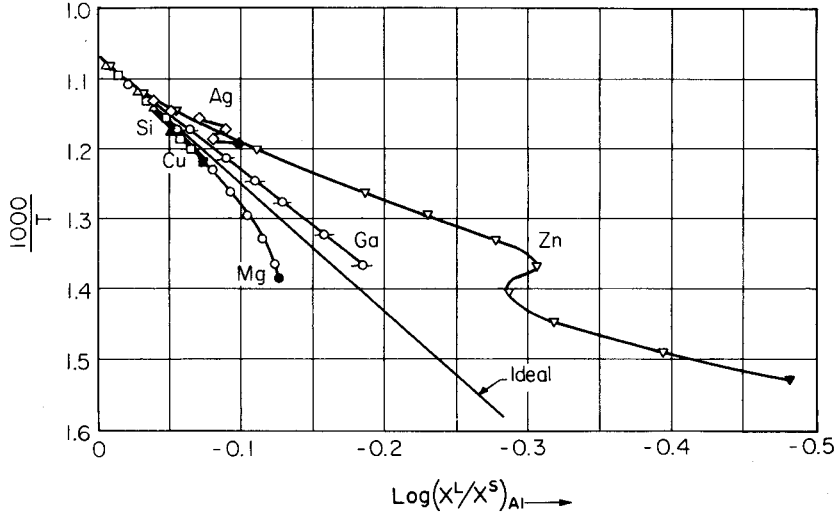

Fig. 6. Equilibrium solidus and liquidus data for binary aluminum alloy systems with extensive solid and liquid solubility plotted according to Eq 7 (Ref 44).

For ideal or real aluminum + B solutions:

$$k = 1 - \frac{m_L \Delta H_{f,Al}}{RT^2_{f,Al}} \qquad \text{(Eq 9)}$$

where m_L is the liquidus slope.

Figure 7 summarizes the effect of relative deviation from ideality on the general form of binary phase diagrams. Aluminum, being trivalent and reactive, forms multiple stable intermetallic compounds of the β-type in Fig. 7(e). This leads to complex phase diagrams and low solid solubility, the prerequisite for commercially useful age hardening.

Solvus. Thermodynamic analysis of the solvus curve, the locus of maximum solid solubility in the aluminum-rich phase, is more complex than for liquidus and solidus. Its very existence implies considerable deviation from ideality. Considering two-phase equilibrium between α and intermetallic compound β, the usual situation in age-hardening alloys, $\mu^B_\alpha = \mu^B_\beta$, $a^B_\alpha = a^B_\beta$. By making suitable assumptions ($a^B_\alpha = \gamma^B_\alpha X^B_\alpha$ where γ^B_α, the Henry's law activity coefficient, is independent of temperature

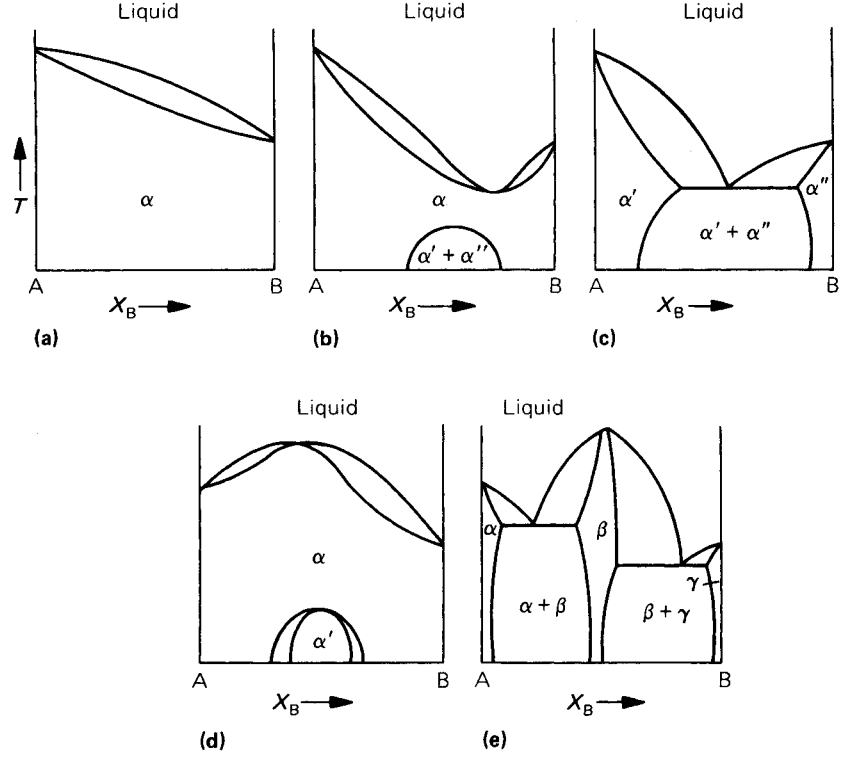

Fig. 7. The effect of relative deviation from ideality on the general form of binary phase diagrams: (a) phase diagram for ideal solutions; (b) phase diagram for case where $\Delta H^S_m > \Delta H^L_m > 0$ (m denotes mixing); (c) same as (b) except ΔH_m is more positive; (d) phase diagram for case where $\Delta H^S_m < \Delta H^L_m < 0$; (e) same as (b) except that ΔH_m is more negative (Ref 41).

and composition and $a_\beta^B = X_\beta^B$ in an ideal solution), Ref 41 shows that:

$$ln \frac{X_\alpha^B}{X_\beta^B} = \frac{\Delta \bar{S}_{v,\alpha}^B}{R} - \frac{\Delta \bar{H}_\alpha^B}{RT} \quad \text{(Eq 10)}$$

$\Delta \bar{S}_{v,\alpha}^B$ is the relative vibrational entropy change corresponding to the transfer of 1 mole of B from the pure state to α, $\Delta \bar{H}_\alpha^B$ is the relative partial molar enthalpy change of B in α; there is close similarity to Eq 7. Assuming that the β-phase is very stable and concentrated in B so that X_β^B is independent of temperature and close to unity, the relationship can be tested by plotting $1/T$ against log X_α^B; the result should be a straight line of slope $-2.303R/\Delta \bar{H}_\alpha^B$ and intercept on the concentration axis of $\Delta \bar{S}_{v,\alpha}^B/2.303R$. This is shown for a representative series of solutes in Fig. 8. There is reasonable agreement for the transition metals and at higher concentrations for silicon and copper. In general, the larger $\Delta \bar{H}_\alpha^B$, the higher is $\Delta \bar{S}_{v,\alpha}^B$. The most important contribution to solution enthalpy is strain energy; this is associated with a reduction in the local vibrational frequencies giving rise to increased solution entropy. Table 2 gives experimental values of $\Delta \bar{H}_\alpha^B$.

Strain energy is dependent on the difference of radius between solvent and solute. A measure of lattice strain is the variation of lattice parameter with concentration of solute; these data are also summarized in Table 2. In the absence of the formation of a stable compound, extensive solid solution is only achieved when there is $\lesssim$15% difference in atomic radii (Ref 8). Also summarized in Table 2 are resistivity increments and the atomic percents of solutes. These can vary widely and show period re-

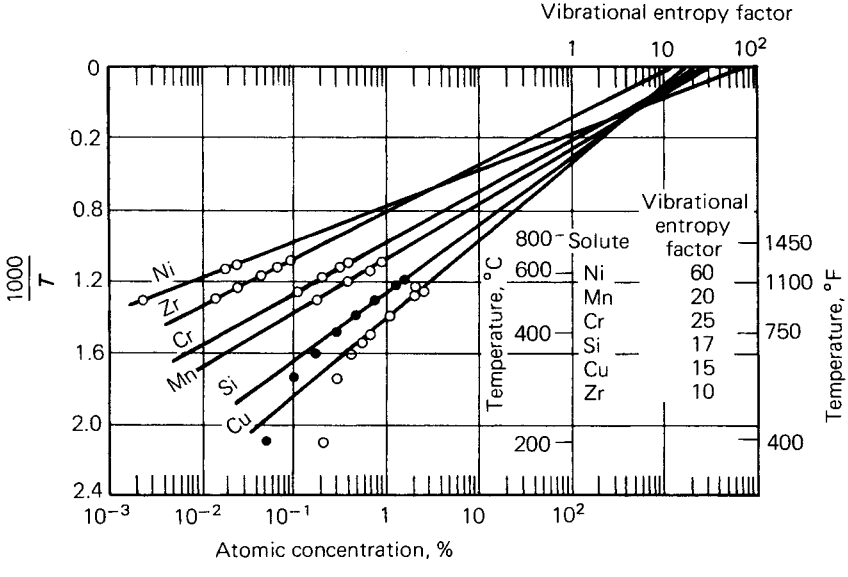

Fig.8. Equilibrium solvus data for selected binary aluminum alloy systems plotted according to Eq 10 so as to obtain relative partial molar solution enthalpy and entropy changes (Ref 50).

lationships associated with the variation of outer electronic structure of solvent and solute (Ref 44 and 45).

Ternary alloys with second phases of well-defined two- or three-component stoichiometry can be analyzed as pseudobinary through use of the equilibrium constant. In the general two-component case, $\beta = B_nC_n$, for example Mg_2Si and $MgZn_2$:

$$K = (a_\alpha^B)^n(a_\alpha^C)^m/(a_\beta^B)^n(a_\beta^C)^m$$

If activity coefficients in α are constant we can define $K' = (X_\alpha^B)^n(X_\alpha^C)^m$ and use Eq 10 to calculate:

$$lnK' = \frac{-\Delta\tilde{H}_\alpha^\beta}{RT} + \text{constant} \qquad \text{(Eq 11)}$$

$\Delta\tilde{H}_\alpha^\beta$ is the solution enthalpy of β in α.

Representative data are shown in Fig. 9 for alloys on the α-β tie line, and show reasonable agreement. This principle can be extended to off-stoichiometric alloy compositions because K' is constant for any particular temperature. From the definition of K', the following equation results:

$$\log X_\alpha^B = \log K' - \frac{m}{n}\log X_\alpha^C \qquad \text{(Eq 12)}$$

Thus, a logarithmic plot of X_α^B against X_α^C for any particular temperature should be linear with slope $-m/n$. An example is shown in Fig. 10 for the aluminum-magnesium-zinc system. The $\log X_\alpha^{Mg} - \log X_\alpha^{Zn}$ isotherms show a distinct change of slope as the stoichiometric composition of the equilibrium phase changes. Deviation from the expected slope of -2 for the $MgZn_2$ solvus is probably associated with systematic deviation from ideality with increased zinc concentration.

The Metastable Solvus. Age hardening is generally accomplished through the precipitation of a metastable variant of the equilibrium phase,

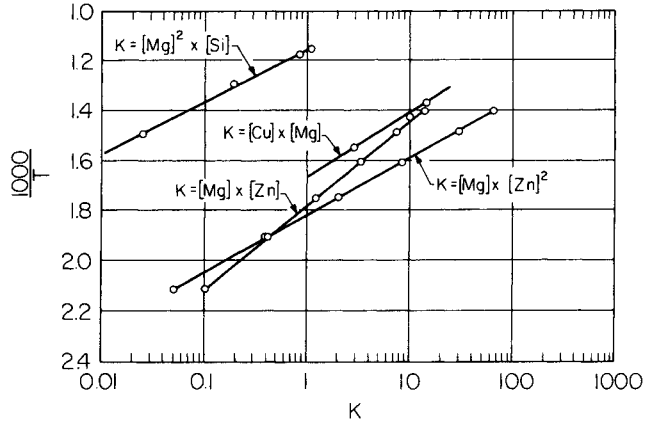

Fig. 9. Equilibrium pseudobinary solvus data for selected ternary aluminum alloy systems plotted according to Eq 11 to show how the equilibrium constant can be used to obtain the molar solution enthalpy of compound second phases (Ref 44).

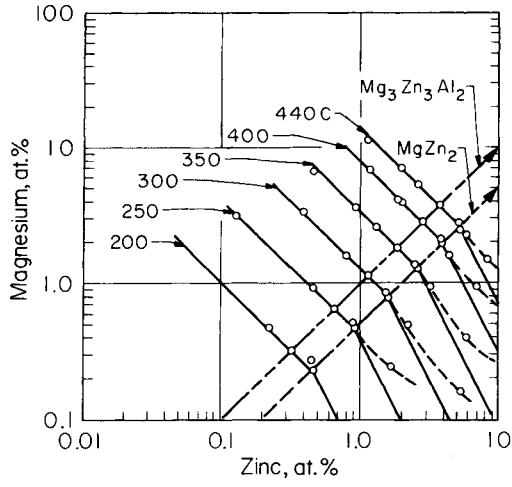

Fig. 10. Equilibrium solvus isotherms for the aluminum-rich corner of the aluminum-magnesium-zinc system plotted according to Eq 12 to show the effect of excess magnesium or zinc (Ref 44).

β' instead of β. The surface free energy change that accompanies the generation of new interfaces is minimized by structural rearrangement to give good precipitate and matrix lattice matching, but at the expense of volumetric free energy. By definition, ΔG for a metastable phase is less negative than that of the equilibrium phase. For metastable equilibrium $\alpha + \beta'$, $\mu_\alpha^B = \mu_{\beta'}^B > \mu_\beta^B$, the metastable solvus is shifted to higher concentration than the equilibrium solvus.

Because there can be more than one metastable variant, there can be more than one metastable solvus. Multiple structural rearrangement of this type is a feature of commercially useful, age-hardening alloy systems and often leads to difficulty in establishing the equilibrium phase relationship. Figure 11 shows metastable solvus curves in the aluminum-copper system.

Prediction of Phase Diagrams from Thermodynamic Data. In the past decade, considerable advances have been made in the thermodynamic evaluation of phase diagrams, particularly through the application of computer techniques (Ref 46). The available data and computational procedures have been systemized internationally since 1971 through the CALPHAD (Computer Coupling of Phase Diagrams and Thermochemistry) project (Ref 47) (Calculation of Phase Diagrams). Application for multicomponent aluminum alloy phase diagram prediction has some inherent problems, particularly regarding the unexpected occurrence of ternary intermetallic phases, but is rapidly becoming an effective procedure.

Prediction of the behavior of multicomponent systems requires explicit equations that describe the absolute free energy of all principal phases in the relevant binary systems as a function of composition and temperature. Solution phases are analyzed in terms of this deviation from ideality, and compound phases are analyzed as a function of stoichiometry. Critically

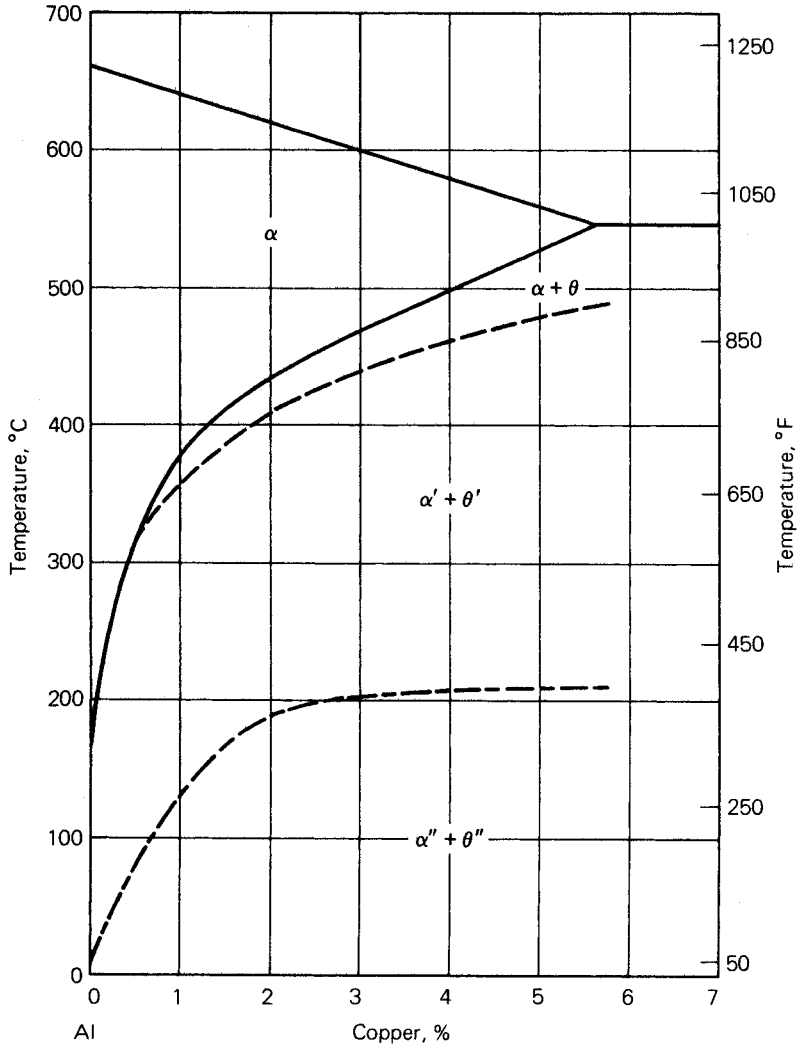

Fig. 11. Metastable equilibrium solvus curves for aluminum-rich aluminum-copper alloys (Ref 51).

assessed thermodynamic data are available in database form (ALLOYDATA) (Ref 48).

Ternary phase diagrams are calculated as isothermal sections by minimizing the Gibbs free energy of the system for progressive pair-wise combination of the available phases and by determining the most stable phase configuration. The calculated phase compositions show the positions of the phase boundaries. Once the generalized topographical form of the phase diagram is established, relatively few experiments are needed to test the validity. To date (1980), the following ternary aluminum-

containing systems have been examined: Al-Fe-Ti, Al-Ga-Ge, Al-Ga-In, Al-Ge-Sn, Al-Li-Mg, and Al-Ni-Ti.

As well as the 15 binaries required for these systems, phase diagrams of the following binary systems have also been examined: Al-Ca, Al-Ce, Al-Co, Al-Cr, Al-Cu, Al-Mn, Al-Mo, Al-Nb, Al-O, Al-P, and Al-Si (Ref 49). In principle, any ternary or quaternary combination of these binary systems can be analyzed.

MAJOR ALLOY SYSTEMS

Aluminum-Copper. Copper is one of the most important alloying elements for aluminum, because of its appreciable solubility and strengthening effect. Many commercial alloys contain copper, either as the major addition or among the principal alloying elements, in concentrations of 1 to 10%. It is used frequently in combination with magnesium.

The aluminum-copper system has been reviewed in detail (Ref 6). The aluminum-rich end of the phase diagram is eutectic Al-$CuAl_2$. The eutectic temperature is 548 °C (1018 °F), and the composition of the eutectic liquid is aluminum-33.2 wt% copper in equilibrium with an aluminum-solid solution containing 5.7 wt% copper (2.53 at.%). The $CuAl_2$ intermetallic phase has a range of composition from 52.5 to 53.7 wt% copper at the eutectic temperature, and from 53.2 to 53.9 wt% at 400 °C (750 °F), compositions slightly deficient in copper for the quoted stoichiometry.

The precipitation reactions are as follows (Ref 51): supersaturated solid solution → coherent platelike GP (Guinier-Preston) zones $/\!/\{001\}_{Al}$ → coherent platelike $\theta''/\!/\{001\}_{Al}$ → semicoherent platelike $\theta'/\!/\{001\}_{Al}$ → noncoherent θ. Structures of these phases are given in Table 3.

Aluminum-Lithium. Binary aluminum-lithium alloys offer interesting combinations of low-density and high-elastic modulus. In aluminum-rich alloys, the eutectic composition is 9.9% lithium and the eutectic temperature is 600 °C (1110 °F). Lithium has significant solubility in aluminum (5.2% max), and the binary alloys show appreciable precipitation hardening. The strengthening precipitate comes from Al_3Li, which is a metastable, ordered δ' phase.

Aluminum-Magnesium. Binary aluminum-magnesium alloys are the basis for an important class of non-heat treatable alloys (5XXX series alloys). Although magnesium has substantial solubility in solid aluminum, binary alloys do not show appreciable precipitation-hardening characteristics with concentrations below 7% magnesium. Magnesium, however, does provide substantial strengthening with good ductility as a result of cold work, in addition to excellent corrosion resistance and weldability.

In aluminum-rich alloys, the eutectic temperature is 450 °C (840 °F) and the concentration is 35% magnesium. The phase in equilibrium with aluminum is usually given as Mg_2Al_3 (37.3% magnesium), although this composition is outside the limits of existence (34.8 to 37.1%) (Ref 52). The formula Mg_5Al_8 (36% magnesium) fits the composition of the solid phase and most of the proposed structures. Equilibrium in solidification

is obtained only with cooling rates of less than 5×10^{-6} °C/h (9×10^{-6} °F/h) (Ref 53). Solidification under nonequilibrium conditions leads to coring, with the Mg_5Al_8 phase appearing at magnesium contents as low as 4 to 5% magnesium (Ref 54). Mg_5Al_8 is very brittle below 330 °C (630 °F), but shows some plasticity at higher temperatures (Ref 55).

Aluminum-Manganese. Non-heat treatable alloys containing slightly over 1% manganese, for example 3003 alloy, are of considerable commercial importance. Manganese is also widely used in lesser amounts as an alloying addition in heat treatable alloys such as 2024 alloy with 0.30 to 0.9% manganese, and non-heat treatable alloys such as 5182 alloy with 0.20 to 0.50% manganese. In general, manganese increases the strength of wrought alloys. However, manganese present as undissolved intermetallic compounds usually has the effect of decreasing ductility. Another important effect of manganese on aluminum and its alloys is to reduce the susceptibility to intergranular or stress corrosion.

In the binary system, manganese has only a slight effect in lowering the freezing point of aluminum. The eutectic temperature and concentration are 660 °C (1220 °F) and 1.9% manganese (Ref 56). The solid solubility limit of manganese in aluminum is 1.8% at the eutectic temperature. The intermetallic phase, which exists in equilibrium with the aluminum solid solution, has a composition closely corresponding to the formula $MnAl_6$. $MnAl_6$ separates as primary phase from liquid solution containing 1.9 to 4.1% manganese. From solutions of higher concentration, it is formed by peritectic reaction between $MnAl_4$ and liquid at 710 °C (1310 °F).

The only metastable phase that is definitely established for aluminum-manganese alloys has the composition of $MnAl_{12}$ with 14.5% manganese (Ref 57). Iron and silicon >0.2% suppress the formation of $MnAl_{12}$; chromium, on the other hand, stabilizes it (Ref 58). In the aluminum-manganese-chromium system, there is a ternary phase that forms only in the solid state by peritectoid reaction at 590 °C (1090 °F). This phase forms $(CrMn)Al_{12}$ with a range of composition from 2% chromium, 12% manganese to 4% chromium, 10% manganese (Ref 57). This ternary phase is isomorphous with the $MnAl_{12}$ phase.

Aluminum-Silicon. The commercial importance of aluminum-silicon alloys is based on their high fluidity and low shrinkage in casting, brazing, and welding applications. The hardness of silicon particles imparts wear resistance. Modification with sodium or strontium (<0.02%) results in a fine distribution of silicon particles in hypoeutectic alloys. Alternatively, phosphorous (<0.01%) can be added as a nucleating agent for hypereutectic alloys.

The aluminum-silicon system forms a simple eutectic with limited solid solubility at both ends. The eutectic occurs at 580 °C (1080 °F) and 12.5% silicon (Ref 6). At the eutectic temperature, the aluminum and silicon solid solutions contain 1.65% silicon and about 0.5% aluminum, respectively. Other intermetallics do not exist in the pure binary system.

Aluminum-Zinc. The aluminum-zinc binary alloys were among the first aluminum alloys commercially developed, but have been largely displaced by aluminum-copper and aluminum-silicon. Aluminum-zinc alloys are primarily used for electrolytic protection against corrosion. Super-

plasticity observed near the aluminum-zinc eutectoid (Ref 59, 60) offers the prospect for expanded commercial application. Currently, zinc is usually used with magnesium and copper in wrought products.

Zinc forms a eutectic-type system with aluminum. The eutectic reaction occurs at 380 °C (720 °F), with liquid containing 94.9% zinc reacting to form aluminum solid solution containing 82.8% zinc and zinc solid solution containing 1.1% aluminum.

A miscibility gap exists in the aluminum solid solution, resulting in a monotectoid reaction at 275 °C (530 °F) between aluminum solid solutions containing 78 and 31.6% zinc and zinc solid solution containing 0.6% aluminum. The solubility gap disappears at 60% zinc and 351.5 °C (664.7 °F), at 61.3% zinc. A eutectoid occurs at 78% zinc and 275 °C (530 °F).

Aluminum-Copper-Lithium. The addition of copper to aluminum-lithium binary alloys reduces the solubility significantly beyond about 1.5% lithium at 515 °C (960 °F). In the aluminum-rich end of the phase diagram, there are three compounds in equilibrium with aluminum: T_B, T_1, and T_2. The T_B phase is Cu_4LiAl_7, corresponding to 56.5% copper, 1.5% lithium. Its structure is similar to that of $\theta'(CuAl_2)$ phase formed in age-hardenable aluminum-copper alloys. The T_1 phase is $CuLiAl_2$ containing approximately 52.8% copper and 5.4% lithium. The T_2 phase has a composition close to $CuLi_3Al_6$ (26.9% copper, 8.8% lithium). Depending on the composition and temperature, the relative amounts of different phases of δ' and T-phases can be varied to obtain different mechanical properties.

Aluminum-Copper-Silicon (Ref 61). Several commercial aluminum-based casting alloys contain both copper and silicon as major alloying ingredients. Hot shortness in casting or welding aluminum-copper-silicon alloys is strongly dependent on composition. Hot shortness is maximum at the limit of solid solubility when the amount of eutectic present is at a minimum.

No ternary compounds are formed; the phases in equilibrium with aluminum are $CuAl_2$ and silicon. An alloy of eutectic composition contains 26 to 31% copper and 5 to 6.5% silicon and solidifies at 520 to 525 °C (970 to 975 °F). The solid solubility of silicon in $CuAl_2$, or of copper and aluminum jointly in silicon, is believed to be extremely small. In an aluminum solid solution, the presence of a second dissolved element usually reduces the solubility of the first, and vice versa. Nonequilibrium freezing, even by quenching from the liquid, has little effect on the structure of the alloys.

Aluminum-Copper-Magnesium (-Silicon). Commercial alloys containing both copper and magnesium as major additions also contain sufficient silicon to give them the characteristics of quaternary alloys rather than ternary alloys. The principal precipitation-hardening reactions, however, are those of the ternary aluminum-copper-magnesium system.

The commercially important alloys contain copper as major addition, and the phase reactions which occur are those between an aluminum solid solution and the intermetallic phases $CuAl_2$ and $CuMgAl_2$. At 510 °C (950 °F), a ternary eutectic reaction occurs between liquid containing 33.1% copper and 6.25% magnesium, $CuAl_2$, $CuMgAl_2$, and aluminum solid solution containing 4.28% copper and 1.35% magnesium. A quasibinary

section also exists with a eutectic at 520 °C (970 °F), at which a liquid phase with 24.5% copper and 10.5% magnesium reacts to form the solid phases $CuMgAl_2$ and aluminum solid solution containing 2.9% copper and 2.9% magnesium. Precipitation hardening at high ratios of copper to magnesium is achieved in the sequence GP zones through a coherent phase (θ′) to $CuAl_2$ (θ). Precipitation hardening at lower ratios of copper to magnesium is achieved in the sequence GP zones through a coherent phase to $CuMgAl_2$.

The addition of silicon to the system results in the appearance of three quaternary invariant reactions for compositions of commercial alloys. These are:

$$L \rightarrow (Al) + CuAl_2 + CuMgAl_2 + Mg_2Si \text{ at } 505\ °C\ (940\ °F)$$

$$L \rightarrow (Al) + CuAl_2 + Al_4CuMg_5Si_4 + Si \text{ at } 510\ °C\ (950\ °F)$$

$$L + Mg_2Si \rightleftharpoons (Al) + CuAl_2 + Al_4CuMg_5Si_4 \text{ at } 510\ °C\ (950\ °F)$$

As nonequilibrium eutectics after solidification, these reactions limit temperatures for ingot homogenization. In the higher strength alloys, these may be equilibrium reactions and may place an upper limit on temperatures for solution heat treatment.

Precipitation reactions involving silicon, Mg_2Si, or the Q-phase ($Al_4CuMg_5Si_4$) may occur at some compositions, but are not major contributors to hardening in the alloys with copper as major element. The iron and manganese in commercial aluminum-copper-magnesium-silicon alloys perform important functions in yielding constituents and dispersoids. By forming insoluble phases with copper and silicon, they reduce the amounts of copper and silicon available for the aluminum-copper-magnesium-silicon phase reactions.

Aluminum-Magnesium-Silicon. The aluminum-magnesium-silicon system is the basis of a major class of heat treatable alloys used for both wrought and cast products. These alloys combine many favorable characteristics, including moderately high strength, relatively low quench sensitivity, and good corrosion resistance. The more dilute alloys are used frequently for architectural applications, usually in the form of extruded sections which are given no separate solution heat treatment before artificial aging.

The equilibrium-phase diagram is relatively simple and well established. The system is pseudobinary Al—Mg_2Si at magnesium to silicon ratios of 1.73-to-1 (wt%). The pseudobinary eutectic horizontal is at 595 °C (1100 °F). The composition of the eutectic liquid is 8.15 wt% magnesium and 4.75 wt% silicon in equilibrium with aluminum solid solution containing 1.13 wt% magnesium and 0.67 wt% silicon (~1.85 wt% Mg_2Si). By dividing the system along this line, the aluminum-rich end can be considered as two simple ternary eutectic systems: Al—Mg_2Al_3—Mg_2Si at 450 °C (840 °F) and Al—Si—Mg_2Si at 555 °C (1030 °F). Solid solubility of Mg_2Si in aluminum is reduced slightly by excess silicon, much more so by excess magnesium. Wrought commercial alloys vary from aluminum ~0.6 wt% Mg_2Si to aluminum 1.5 wt% Mg_2Si with varying degrees of slight magnesium or silicon excess.

The precipitation reactions in this alloy system have been studied in detail (Ref 62–64). The following sequence takes place under normal cir-

cumstances: supersaturated solid solution → semicoherent β″ rods $/\!/\langle 001\rangle_{Al}$ → semicoherent β′ needles $/\!/\langle 001\rangle_{Al}$ → semicoherent β plates $/\!/\langle 001\rangle_{Al}$ → noncoherent βMg_2Si. It is thought that the β″ phase has the same structure as $\beta' Mg_2Si$ but there is some evidence that it contains ~20% Al. Details of the β′ and β structures are given in Table 3.

Aluminum-Magnesium-Lithium. The addition of magnesium to aluminum-lithium binary alloys further reduces density but has little effect on modulus. Magnesium additions reduce the solubility of lithium. Lithium additions restrict the field of existence of Mg_5Al_8 and of the E (AlMg) phase, and expand the $Mg_{17}Al_{12}$ phase field at 470 °C (880 °F). Thus, aluminum is in equilibrium with both Mg_5Al_8 and $Mg_{17}Al_{12}$, along with $LiMgAl_2$ and LiAl. $LiMgAl_2$ ternary phase is formed approximately at 8.5% lithium and 28.2% magnesium. Aging an alloy of 5% magnesium and 2% lithium in the range 130 to 180 °C (270 to 360 °F) gives rise to δ′ (Al_3Li) phase and $LiMgAl_2$. In aluminum-magnesium-lithium alloys, magnesium contributes to strength in two ways. It adds a component of solid solution strengthening and decreases the lithium solubility in aluminum, resulting in increased volume fraction of δ′.

Aluminum-Magnesium-Zinc and Aluminum-Copper-Magnesium-Zinc. Compositions within these systems form important classes of heat treatable alloys and, in the quaternary system, yield the highest strengths known for commercial aluminum alloys. In almost all cases, zinc is the major addition element.

The characteristics of ternary aluminum-zinc-magnesium alloys are influenced by the high solid solubility of both elements. In the ternary system, matrix compositions for invariant reactions are at such high zinc and magnesium levels that nonequilibrium melting is rarely encountered. For commercial compositions, solvus temperatures are generally low in comparison to those in other heat treatable alloy systems.

The phases in equilibrium with an aluminum matrix in commercial alloys are designated $MgZn_2$ (M-phase), $Mg_3Zn_3Al_2$ (T-phase), and Mg_5Al_3 (β-phase). The first phase ranges in composition from $MgZn_2$ to Mg_4Zn_7Al. The T-phase has a wide range of composition, from 74% zinc–16% magnesium to 20% zinc–31% magnesium. The β-phase appears only when the magnesium content is considerably greater than the zinc content. Such alloys are strengthened primarily by magnesium in solid solution.

Precipitation hardening of alloys with zinc in excess of magnesium occurs in the sequence zones through coherent precipitate to the M-phase. If the magnesium content is greater than the zinc content, the sequence is zones through coherent precipitate to the T-phase.

In quaternary alloys containing copper, zinc is the major addition in commercial wrought alloys, and magnesium is usually in excess of copper. The M-phase composition ranges in the quaternary system from $MgZn_2$ to CuMgAl, and may be described as $Mg(Al,Cu,Zn)_2$. The range of composition for the T-phase is from that of the aluminum-magnesium-zinc ternary to that of the phase designated $CuMg_4Al_6$, and may be described as $Mg_3(Al,Cu,Zn)_5$. A third phase in commercial alloys is $CuMgAl_2$ (S-phase), with a small range of composition. The $CuAl_2$ phase appears only if copper is considerably in excess of magnesium.

Several nonequilibrium invariant melting reactions are encountered in the high-strength quaternary alloys. A reaction at 475 °C (890 °F) involving the M-, T-, and S-phases is usually encountered, but as copper content increases, melting may be encountered down to about 460 °C (860 °F). Usually, the J-phase has the highest solvus temperature and is slow to disappear during ingot homogenization.

Precipitation hardening in high-strength alloys is by the sequence leading to M-phase. Zones and coherent precipitates are low in copper content, and precipitates increase in copper content in the overaging regime. Additions of iron, manganese, and silicon interact with one another and with copper and magnesium. Chromium reacts with aluminum and magnesium to form a dispersoid.

LOW LEVEL ALLOY SYSTEMS

Aluminum-Boron. Small amounts of boron (<0.1%) are added to aluminum alloys primarily to either refine the grain size, or increase the electrical conductivity by precipitating titanium and/or vanadium from liquid solution. There is a eutectic at 0.022% boron, 660 °C (1220 °F) between aluminum and B_2Al. The solid solubility of boron in aluminum is negligible. B_2Al forms by peritectic reaction at 980 °C (1800 °F) from $B_{12}Al$ (Ref 66).

Aluminum-Chromium. Chromium, in small amounts (<0.35%), is added to numerous commercial aluminum alloys. Chromium additions tend to raise the recrystallization temperature, and may also be used to produce a gold color upon anodizing. Above 0.4% chromium at the aluminum end of the aluminum-chromium equilibrium diagram, a constituent corresponding to the formula $CrAl_7$ reacts peritectically to form the aluminum-rich solid solution (Ref 67). The solid solubility of chromium in aluminum is quite low, decreasing from 0.8% at 660 °C (1220 °F) to 0.30% at 430 °C (810 °F). $CrAl_7$ reportedly ceases to be primary at about 2.5% chromium and 790 °C (1450 °F). It is replaced by a constituent having the formula Cr_2Al_{11} (Ref 68).

Aluminum-Iron (Ref 69). Iron is the dominant impurity in virtually all commercial aluminum alloys. Some iron may be added intentionally, although the total content is usually kept below 1.0%. There is a eutectic in aluminum-rich alloys at 655 °C (1210 °F) with a probable composition within the range 1.7 to 2.2% iron. The phase in equilibrium with aluminum is usually designated as $FeAl_3$ (40.7% iron), although some analysis of crystals extracted from alloys are close to Fe_2Al_7 (37.3% iron). The $FeAl_3$ compound forms directly from the liquid at 1150 °C (2100 °F) and not by peritectic reaction. In rapidly chilled alloy, the metastable compound $FeAl_6$ (22.6% iron) is produced.

Aluminum-Titanium. Titanium is a normal impurity in aluminum, originating from TiO_2, which is present in most bauxites. It is also a

common addition to most commercial alloys because it is a very effective grain refiner during casting. In aluminum-rich alloys, the eutectic temperature and concentration are 665 °C (1230 °F) and 0.12 to 0.15% titanium. The phase coexisting with aluminum corresponds to the formula $TiAl_3$ (37.2% titanium), which has a range of existence from 36.5 to 37.5% titanium and is formed by peritectic reaction (Ref 70).

Aluminum-Vanadium (Ref 71). Vanadium is a minor impurity in aluminum, originating in most cases from bauxite. Mechanical properties of aluminum and aluminum alloys are not increased substantially by vanadium or ferro-vanadium additions. The limited increase in strength resulting from small additions is largely because of the grain refining effect of vanadium, rather than any intrinsic strengthening.

VAl_{10} (15.8% vanadium), which has a range of existence from 15.1% vanadium (V_2Al_{21}) to 15.9% vanadium, forms by peritectic reaction at approximately 670 °C (1240 °F) from the liquid phase and a phase which can be designated as VAl_7 or V_7Al_{45}. V_7Al_{45} if formed by peritectic reaction at approximately 690 °C (1270 °F) from VAl_6. VAl_6, also given as V_4Al_{23}, is formed by peritectic reaction at 735 °C (1360 °F) from VAl_3.

Aluminum-Zirconium. Zirconium is a minor addition to certain aluminum-magnesium-zinc alloys such as 7005, in which it may reduce stress corrosion susceptibility. It also imparts a grain refining effect to many aluminum alloys, but is not commercially used for this purpose. The equilibrium diagram for aluminum-rich alloys of this system is of the peritectic type. The peritectic horizontal lies at 660 °C (1220 °F), the reactant being $ZrAl_3$ and the resultant an aluminum-rich solid solution containing a maximum of 0.28% zirconium. The break in the liquidus curve, at the end of the peritectic horizontal, lies at 0.11% zirconium. The solid solubility of zirconium in aluminum decreases with falling temperature and lies at about 0.05% at 500 °C (930 °F) (Ref 72).

Aluminum-Iron-Silicon (Ref 73). Iron and silicon are the most common impurities in both commercial wrought and cast aluminum alloys. Two ternary phases that can be in equilibrium with aluminum are Fe_2SiAl_8 (α) and $FeSiAl_5$ (β). Another phase, $FeSiAl_4$ (δ), is often present in high silicon alloys, and a fourth phase, $FeSiAl_3$ (γ), forms in high iron and high silicon alloys.

$FeSiAl_8$ (31.6% iron, 7.8% silicon) is the phase that appears as Chinese script (often reported as Fe_3SiAl_{12}). $FeSiAl_5$ (25.6% iron, 12.8% silicon) forms very thin platelets that in section appear as long needles. Most commercial alloys are not in equilibrium and often alloys in which $FeAl_6$, $FeAl_3$, Fe_2SiAl_8, $FeSiAl_6$, and $FeSi_2Al_4$ coexist with one another and with silicon are produced. In heat treated alloys, equilibrium may often be reached by diffusion in the solid state, and $FeSiAl_5$ may be found in the Chinese script shape characteristic of Fe_2SiAl_8 or in the platelet form characteristic of $FeSi_2Al_4$. Thus, identification of the phases by shape alone may be misleading.

REFERENCES

1. L.W. Eastwood, *Gases in Non-Ferrous Metals and Alloys,* American Society for Metals, 1953
2. L.P. Costas and R.P. Marshall, The Solubility of Lithium in Aluminum, *Transactions of AIME,* Vol 224, 1962, p 970–974
3. E.D. Levine and E.J. Rapperport, *The Aluminum-Lithium Phase Diagram,* U.S. Atomic Energy Commission, Division of Technical Information, 6 Feb 1962
4. W.R.D. Jones and P.P. Das, The Solid Solubility of Lithium in Aluminum, *Journal of the Institute of Metals,* Vol 87, 1958–1959, p 338–340
5. W.B. Pearson, *Handbook of Lattice Spacings and Structures of Metals and Alloys,* Vol 2, Oxford: Pergamon Press, 1967
6. L.F. Mondolfo, *Aluminum Alloys: Structure and Properties,* London: Butterworths, 1976
7. D. Munson, *Journal of the Institute of Metals,* Vol 95, 1967, p 217–219
8. W. Hume-Rothery and G.V. Raynor, *The Structure of Metals and Alloys,* London: The Institute of Metals, 1962
9. P.J. Black, *Acta Metallurgica,* Vol 4, 1956, p 172–178
10. M.C. Flemings, *Solidification Processing,* New York: McGraw-Hill, 1974
11. J.W. Cahn, S.R. Coriell, and W.J. Boettinger, Rapid Solidification, in *Laser and Electron Beam Processing of Material,* Edited by C.W. White and P.S. Peercy, New York: Academic Press, 1980
12. A.B. Michael and M.B. Bever, *Transactions of AIME,* Jan 1954, p 47
13. S.N. Singh and M.C. Flemings, *Transactions of AIME,* Jan 1969, p 1803
14. T.F. Bower, H.D. Brody, and M.C. Flemings, *Transactions of AIME,* Vol 236, 1966, p 624
15. R.E. Spear and G.R. Gardner, *Transactions of American Foundrymens Society,* Vol 71, 1963, p 209
16. G.R. Armstrong and H. Jones, *Solidification and Casting,* Proceeding of Conference at University of Sheffield, London: Metals Society, 1979
17. P. Ramachandrarao, M.G. Scott, and G.A. Chadwick, *Philosophical Magazine,* Vol 25, 1972, p 961
18. H. Matyja, B.C. Giessen, and N.J. Grant, *Journal of the Institute of Metals,* Vol 96, 1968, p 30
19. J.A. McComb, S. Nenno, and M. Meshii, *Journal of the Physical Society of Japan,* Vol 19, 1964, p 1691
20. C. Suryanarayana and T.R. Anantharaman, *Journal of Materials Science,* Vol 5, 1970, p 992
21. H.A. Davies and J.B. Hull, *Journal of Materials Science,* Vol 9, 1974, p 707
22. N.J. Grant, *Rapid Solidification Processing,* edited by R. Mehrabian, B.H. Kear, and M. Cohen, Baton Rouge, LA: Claitor Publishing Division, 1970, p 230

23. J.A. Horwath and L.F. Mondolfo, *Acta Metallurgica,* Vol 10, 1962, p 1037

24. C.F. Dixon and H.M. Skelly, *International Journal of Powder Metallurgy,* Vol 7 (No. 3), 1971, p 47

25. R.J. Town, *Metal Progress,* Vol 73 (No. 5), 1958, p 70

26. G. Thursfield and M.J. Stowell, *Journal of Materials Science,* Vol 6, 1971, p 1111

27. C. Panseri and M. Paganelli, *Alluminio,* Vol 36, 1967, p 179

28. P.G. Boswell and G.A. Chadwick, *Scripta Metallurgica,* Vol 11, 1977, p 11

29. T.R. Anatharaman and C. Suryanarayana, *Journal of Materials Science,* Vol 6, 1971, p 1111

30. H. Jones, *Aluminum,* Vol 54 (No. 4), 1978, p 274

31. K.O. Krishnanand and R.W. Cahn in *Rapidly Quenched Metals,* edited by N.J. Grant and B.C. Giessen, Cambridge, MA: MIT Press, 1976, p 67

32. R.K. Linde, *Transactions of AIME,* Vol 236, 1966, p 58

33. J.V. Wood and R.W.K. Honeycombe, *Journal of Materials Science,* Vol 9, 1974, p 1183

34. P.E. Brown and C.M. Adams, *Transactions of American Foundrymens Society,* Vol 69, 1961, p 879

35. T. Kattamis and R. Mehrabian, *Journal of Vacuum Science and Technology,* Vol 11 (No. 6), 1974, p 1118

36. H. Jones, *Metallography,* Vol 3 (No. 3), 1970, p 307

37. H. Jones, *Material Science and Engineering,* Vol 5, 1969–1970, p 1

38. D.B. Williams and J.W. Edington, High Resolution Microanalysis and Microstructural Characteristics of Splat Quenched Aluminum-Copper Alloys, in *Rapidly Quenched Metals,* edited by N.J. Grant and B.C. Giessen, Cambridge, MA: MIT Press, 1976, p 135

39. H.A. Davies and J.B. Hull, Some Aspects of Splat Quenching in an Inert Atmosphere and of the Formation of Non-Crystalline Phases in Al-17.3 at. percent Copper, Germanium and Tellurium, *Journal of Materials Science,* Vol 9, 1975, p 707

40. M.G. Scott and J.A. Leake, Formation and Decomposition of an A1-17.3 at. percent Cu Solid Solution, *Acta Metallurgica,* Vol 27, 1975, p 503

41. R.A. Swalin, *Thermodynamics of Solids,* New York: John Wiley & Sons, 1962

42. M.C. Flemings, *Solidification Processing,* New York: McGraw-Hill, 1974

43. K.S. Pitzer and L. Brewer, *Thermodynamics* (revision of Lewis and Randall), New York: McGraw-Hill, 1961

44. L.A. Willey, *Aluminum,* Vol 1, American Society for Metals, 1967

45. M. Mugahid and N.N. Engel, *Scripta Metallurgica,* Vol 13, 1979

46. F.L. Kaufman and H. Bernstein, *Computer Calculation of Phase Diagrams,* New York: Academic Press, 1970

47. L. Kaufman, Ed., CALPHAD: Computer Coupling of Phase Diagrams and Thermochemistry, Manlabs Inc., Cambridge, MA

48. ALLOYDATA: Division of Chemical Standards, National Physical Laboratory, Teddington, Middlesex, U.K.

49. Published in CALPHAD, New York: Pergamon Press, 1976–1980

50. C. Zener, *Thermodynamics in Physical Metallurgy,* American Society for Metals, 1950

51. E. Hornbogen, *Aluminium,* Vol 43, 1967, p 115

52. L.F. Mondolfo, *Aluminum Alloys: Structure and Properties,* London: Butterworths, 1976, p 312

53. J. Guillet, *et al,* Influence of Cooling Rate on the Condition of Solid Solutions After Annealing, *Memoire Scientifique de la Revue de Metallurgic,* Vol 67 (No. 9), June 1970, p 377 (French)

54. R.D. Vengrenovich, *et al,* Changes in Composition of Solid Solutions during Non-equilibrium Crystallization of Aluminum-Base Binary Alloys, *Zhurnal Fizicheskoi Khimii,* Vol 44 (No. 8), Aug 1970, p 1979 (Russian)

55. E.M. Savitsky, *et al, Journal of the Institute of Metals,* Vol 253 (No. 20.81), p 1002

56. L.F. Mondolfo, *Manganese in Aluminum Alloys,* the Manganese Center, 1978, p 4

57. L.F. Mondolfo, *Manganese in Aluminum Alloys,* the Manganese Center, 1978, p 29

58. L.F. Mondolfo, *Manganese in Aluminum Alloys,* the Manganese Center, 1978, p 326

59. W.A. Backofen, I.R. Turner, and D.H. Avery, *Transactions American Society for Metals,* Vol 57, 1964, p 980

60. S.D. Fields, Jr., *IBM J Res Develop,* Vol 9, 1964, p 134

61. L.F. Mondolfo, *Aluminum Alloys: Structure and Properties,* London: Butterworths, 1976, p 513

62. J.W. Pashley, J.W. Rhodes, and A. Sendorek, *Journal of the Institute of Metals,* Vol 94, 1966, p 41–48

63. M.H. Jacobs, *Philosophical Magazine,* Vol 26, 1972, p 1–13

64. H. Westengen and N. Ryum, *Zeitschrift fuer Metallkunde,* Vol 70, 1979, p 528–535

65. E.D. Boyes, *et al, Institute of Physics—Conference Series,* No. 36, 1977, p 343

66. L.F. Mondolfo, *Aluminum Alloys: Structure and Properties,* London: Butterworths, 1976, p 229

67. H.W.L. Phillips, *Annoted Equilibrium Diagrams of Some Aluminum Alloy Systems,* the Institute of Metals, 1959, p 6

68. L.F. Mondolfo, *Aluminum Alloys: Structure and Properties,* London: Butterworths, 1976, p 249–250

69. L.F. Mondolfo, *Aluminum Alloys: Structure and Properties,* London: Butterworths, 1976, p 283–285

70. L.F. Mondolfo, *Aluminum Alloys: Structure and Properties*, London: Butterworths, 1976, p 385

71. L.F. Mondolfo, *Aluminum Alloys: Structure and Properties*, London: Butterworths, 1976, p 392–393

72. H.W.L. Phillips, *Annotated Equilibrium Diagrams of Some Aluminum Alloy Systems*, The Institute of Metals, 1959, p 20

73. L.F. Mondolfo, *Aluminum Alloys: Structure and Properties*, London: Butterworths, 1976, p 534–536